

Real-space calculation of the conductivity tensor for disordered topological matter

Jose H. García,¹ Lucian Covaci,² and Tatiana G. Rappoport¹

¹*Instituto de Física, Universidade Federal do Rio de Janeiro,
Caixa Postal 68528, 21941-972 Rio de Janeiro RJ, Brazil*

²*Department Fysica, Universiteit Antwerpen, Groenenborgerlaan 171, B-2020 Antwerpen, Belgium*
(Dated: March 23, 2015)

We describe an efficient numerical approach to calculate the longitudinal and transverse Kubo conductivities of large systems using Bastin's formulation [1]. We expand the Green's functions in terms of Chebyshev polynomials and compute the conductivity tensor for any temperature and chemical potential in a single step. To illustrate the power and generality of the approach, we calculate the conductivity tensor for the quantum Hall effect in disordered graphene and analyze the effect of the disorder in a Chern insulator in Haldane's model on a honeycomb lattice.

PACS numbers: 71.23.An,72.15.Rn,71.30.+h

One of the most important experimental probes in condensed matter physics is the electrical response to an external electrical field. In addition to the longitudinal conductivity, in specific circumstances, a system can present a transverse conductivity under an electrical perturbation. The Hall effect [2] and the anomalous Hall effect in magnetic materials [3] are two examples of this type of response. Paramagnetic materials with spin-orbit interaction can also present transverse spin currents [4]. There are also the quantized versions of the three phenomena: while the quantum Hall effect (QHE) was observed more than 30 years ago [5], the quantum spin Hall effect (QSHE) and the quantum anomalous Hall effect (QAHE) could only be observed [6, 7] with the recent discovery of topological insulators, a new class of quantum matter [8].

In the linear response regime, the conductivity tensor can be calculated using the Kubo formalism [9]. The Hall conductivity can be easily obtained in momentum space in terms of the Berry curvature associated with the bands [10]. The downside of working in momentum space, however, is that the robustness of a topological state in the presence of disorder can only be calculated perturbatively [11]. Real-space implementations of the Kubo formalism for the Hall conductivity, on the other hand, allow the incorporation of different types of disorder in varying degrees, while providing flexibility to treat different geometries. Real-space techniques, however, normally require a large computational effort. This has generally restricted their use to either small systems at any temperature [12, 13], or large systems at zero temperature [14].

In this Letter, we propose a new efficient numerical approach to calculate the conductivity tensor in solids. We use a real space implementation of the Kubo formalism where both diagonal and off-diagonal conductivities are treated in the same footing. We adopt a formulation of the Kubo theory that is known as Bastin formula [1] and expand the Green's functions involved in terms of Chebyshev polynomials using the kernel poly-

nomial method [16]. There are few numerical methods that use Chebyshev expansions to calculate the longitudinal DC conductivity [17–20] and transverse conductivity [14, 21] at zero temperature. An advantage of our approach is the possibility of obtaining both conductivities for large systems in a single calculation step, independently of the temperature, chemical potential and for any amount of disorder.

We apply this method to two different systems displaying topological states in a honeycomb lattice. The first one has been extensively explored in the literature [14, 22–24], and consists of disordered graphene under constant perpendicular magnetic field. Our calculation of the longitudinal and Hall conductivities serve to illustrate the key aspects of our approach. We then apply the method to a Chern insulator (CI) in Haldane's model on a honeycomb lattice [25]. This model produces an insulating state with broken time-reversal symmetry in the absence of a macroscopic magnetic field. Instead of behaving as a normal insulator, it exhibits a quantized Hall conductivity $\sigma_{xy} = e^2/h$ in the gapped state. If the inversion symmetry is broken, the system can undergo a topological phase transition to a normal insulator. We investigate the transport properties of Chern insulators and analyze how they are affected by the interplay between disorder and inversion symmetry breaking.

The conductivity tensor can be calculated using the Kubo formula from linear response theory. In the limit $\omega \rightarrow 0$, the elements of the static conductivity tensor for non-interacting electrons are given by the Kubo-Bastin formula for the conductivity [1]

$$\begin{aligned} \tilde{\sigma}_{\alpha\beta}(\mu, T) &= \frac{ie^2\hbar}{\Omega} \int_{-\infty}^{\infty} d\varepsilon f(\varepsilon) \\ &\times \text{Tr} \left\langle v_{\alpha} \delta(\varepsilon - H) v_{\beta} \frac{dG^{+}(\varepsilon)}{d\varepsilon} - v_{\alpha} \frac{dG^{-}(\varepsilon)}{d\varepsilon} v_{\beta} \delta(\varepsilon - H) \right\rangle, \end{aligned} \quad (1)$$

where Ω is the volume, v_{α} is the α component of the velocity operator, $G^{\pm}(\varepsilon, H) = \frac{1}{\varepsilon - H \pm i0}$ are the advanced (+) and retarded (−) Green's functions, and $f(\varepsilon)$ is the

Fermi-Dirac distribution for a given temperature T and chemical potential μ . The expression above was first obtained by Bastin and collaborators in 1971 [1] and later generalized for any independent electron approximation [26]. However, it has not been used often in numerical calculations because of the complications of dealing with an integration in energy. Instead, it is possible to perform analytical integrations by parts [26] to obtain a more treatable expression for the static conductivity at zero temperature, which became known as the Kubo-Streda formula [27]. For the diagonal elements of the conductivity tensor ($\alpha = \beta$), the integration leads to the Kubo-Greenwood formula [15].

Here we propose a new approach to compute, for any finite temperature, both diagonal and off-diagonal conductivities using the Kubo-Bastin formula. Our method consists in expanding the Green's functions in the integrand of eq. (1) in terms of Chebyshev polynomials using the kernel polynomial method [16, 28], a highly efficient and scalable way to calculate the Green's functions in electronic systems [16, 29–31]. For that purpose, we first need to rescale the Hamiltonian so that the upper E^+ and lower E^- bounds of the spectrum are mapped into 1 and -1 respectively. To estimate the bounds, we apply the power method [32], which is normally used to locate dominant eigenvalues in linear algebra. The rescaled Hamiltonian and energy are represented by \tilde{H} and $\tilde{\varepsilon}$ [33] and we can expand the rescaled delta and Green's functions by considering their spectral representations and expanding their eigenvalues in terms of the Chebyshev polynomials:

$$\delta(\tilde{\varepsilon} - \tilde{H}) = \frac{2}{\pi\sqrt{1-\tilde{\varepsilon}^2}} \sum_{m=0}^M g_m \frac{T_m(\tilde{\varepsilon})}{\delta_{m,0} + 1} T_m(\tilde{H}), \quad (2)$$

$$G^\pm(\tilde{\varepsilon}, \tilde{H}) = \mp \frac{2i}{\sqrt{1-\tilde{\varepsilon}^2}} \sum_{m=0}^M g_m \frac{e^{\pm im \arccos(\tilde{\varepsilon})}}{\delta_{m,0} + 1} T_m(\tilde{H}). \quad (3)$$

where $T_m(x) = \cos[m \arccos(x)]$ is the Chebyshev polynomial of the first kind and order m , which is defined according to the recurrence relation $T_m(x) = 2xT_{m-1}(x) - T_{m-2}(x)$. The expansion has a finite number of terms (M) and the truncation gives rise to Gibbs oscillations that can be smoothed with the use of a kernel, given by g_m [16, 28].

Replacing the expansions above in (1) with $\Delta E = E^+ - E^-$, we obtain

$$\sigma_{\alpha\beta}(\mu, T) = \frac{4e^2\hbar}{\pi\Omega} \frac{4}{\Delta E^2} \int_{-1}^1 d\tilde{\varepsilon} \frac{f(\tilde{\varepsilon})}{(1-\tilde{\varepsilon}^2)^2} \sum_{m,n} \Gamma_{nm}(\tilde{\varepsilon}) \mu_{nm}^{\alpha\beta} \quad (4)$$

where $\mu_{mn}^{\alpha\beta} \equiv \frac{g_m g_n}{(1+\delta_{n0})(1+\delta_{m0})} \text{Tr} \left[v_\alpha T_m(\tilde{H}) v_\beta T_n(\tilde{H}) \right]$ does not depend on the energy. Since μ_{mn} involves products of polynomial expansions of the Hamiltonian, its calculation

is responsible for most of the method's computational cost.

On the other hand, $\Gamma_{mn}(\tilde{\varepsilon})$ is a scalar that is energy dependent but independent of the Hamiltonian

$$\Gamma_{mn}(\tilde{\varepsilon}) \equiv [(\tilde{\varepsilon} - im\sqrt{1-\tilde{\varepsilon}^2})e^{im \arccos(\tilde{\varepsilon})} T_m(\tilde{\varepsilon}) + (\tilde{\varepsilon} + im\sqrt{1-\tilde{\varepsilon}^2})e^{-im \arccos(\tilde{\varepsilon})} T_n(\tilde{\varepsilon})]. \quad (5)$$

As shown in (19), once the coefficients μ_{mn} are determined, we can obtain the conductivities for all temperatures and chemical potentials without repeating the most time-consuming part of the calculation [34]. Moreover, the recursive relations between Chebyshev polynomials lead to a recursive multiplication of sparse Hamiltonian matrices that can be performed in a very efficient way in GPUs [20, 29]. Instead of the full calculation of traces, we use self-averaging properties, normally used in Monte-Carlo calculations, to replace the trace in the calculation of μ_{mn} by the average of a small number $R \ll N$ of random phase vectors $|r\rangle$ and further improve the efficiency of the calculation [35, 36]. The conductivities are averaged over several disorder realizations, S , with $R = 5$ for each of them. Because of the self-averaging properties of large systems, the product SR is the main defining factor of the accuracy of the trace operation.

The first problem we apply our method to is the physics of the QHE in disordered graphene. We start from the electronic Hamiltonian of graphene in the presence of a random scalar potential and a perpendicular magnetic field $\mathcal{H} = -t \sum_{\langle i,j \rangle} e^{i\phi_{ij}} c_i^\dagger c_j + \sum_i \varepsilon_i c_i^\dagger c_i$ where c_i is the annihilation operator of electrons on site i where $t \approx 2.8$ eV is the hopping energy between nearest neighbors (NN) sites in a honeycomb lattice. The perpendicular magnetic field is included by Peierls' substitution $\phi_{ij} = 2\pi/\Phi_0 \int_j^i \vec{A} \cdot d\vec{l}$. Using the Landau gauge $\vec{A} = (-By, 0, 0)$, the phase will be $\phi_{ij} = 0$ along the y direction and $\phi_{ij} = \pm\pi(y/a)\Phi/\Phi_0$ along the $\mp x$ direction, where Φ is the magnetic flux per unit cell, Φ_0 being the quantum of magnetic flux. The second term in \mathcal{H} represents the on-site Anderson disorder where ε_i is randomly chosen from a uniform probability distribution $p(\varepsilon_i) = \frac{1}{\gamma} \theta(\frac{\gamma}{2} - |\varepsilon_i|)$, where γ accounts for the amount of disorder introduced in the system. Let us begin with a graphene layer with $N \approx 2.6 \times 10^5$ sites with periodic boundary conditions and weak disorder given by $\gamma = 0.1t$ and $SR = 200$. In the presence of a perpendicular magnetic field such that $\Phi/\Phi_0 \approx 1 \times 10^{-3}$, the electronic density of states (DOS) presents several Landau levels close to the Dirac point. Away from $E = 0$, the magnetic length is larger than the system size; the band structure still presents a large number of peaks, with a non-zero density of states between the peaks, which results in a metal behavior, as seen in Fig. 1 (b). We compute the longitudinal and off-diagonal conductivities as a function of the chemical potential μ and close to $\mu = 0$ the results are consistent with the QHE in pure graphene. Figure

1 (a) shows the peaks in σ_{xx} that are located exactly at the peaks of the density of state. For $\sigma_{xx} = 0$ we see well-resolved plateaus of the Hall conductivity following $\sigma_{xy} = 4e^2/h(n + 1/2)$, indicating that the method captures the topological nature of the insulating phase. The effect of the temperature is the predictable broadening of the longitudinal conductivity peaks together with the smearing of the quantum Hall plateau. Fig. 1 (c) reports Shubnikov-de Haas oscillations in the longitudinal conductivity away from the Dirac point. Similarly to what is observed experimentally [37], they are sensitive to changes in T . To get results as accurate as those in Fig. 1, one needs to look at the convergence of the expansion as a function of the few parameters that were introduced in our approach, such as the polynomial order M and the product SR . To illustrate this, in Fig. 2 we show the dependence of σ_{xx} and σ_{xy} on M and SR . For disordered systems, the interference due to quasi-particle scattering off the impurities [29] results in an oscillatory behavior of the Chebyshev moments. Because of this, an accurate solution requires a large number of moments. The energy resolution of the KPM depends on M and its value is important for the convergence of the sharp peaks of σ_{xx} . This is illustrated in Fig. 2 (a) where the conductivity peak at $E = 0$ is consistent with recent numerical calculations [14, 24] and its convergence is only achieved for $M > 6000$.

The energies of the Landau levels close to the Dirac point scale with \sqrt{n} , reducing the gap between high Landau levels. Simultaneously, the density of states increases with E . Consequently, we need more moments in the expansion to resolve small gaps and localize carriers in

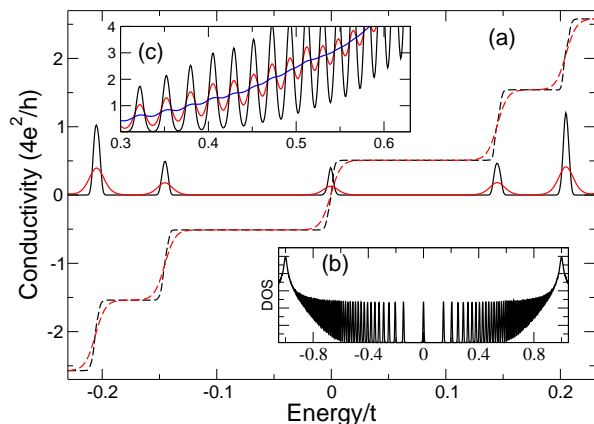


FIG. 1. (a) σ_{xx} (solid line) and σ_{xy} (dashed line) for $k_B T = 0$ (black) and $k_B T/t = 0.004$ (red). (b) Electronic density of states (c) σ_{xx} away from the Dirac point where Shubnikov-de Haas oscillations can be observed for $k_B T/t = 0.002$ (black), $k_B T/t = 0.004$ (red), $k_B T/t = 0.008$ (blue). The parameters in panels (a)-(c) are $\phi/\phi_0 \approx 1 \times 10^{-3}$, $SR = 200$, $M = 6144$ and $N = 2 \times 128 \times 1024$ sites where we use a rectangular geometry to minimize the magnetic flux per unit cell in a system with periodic boundary conditions.

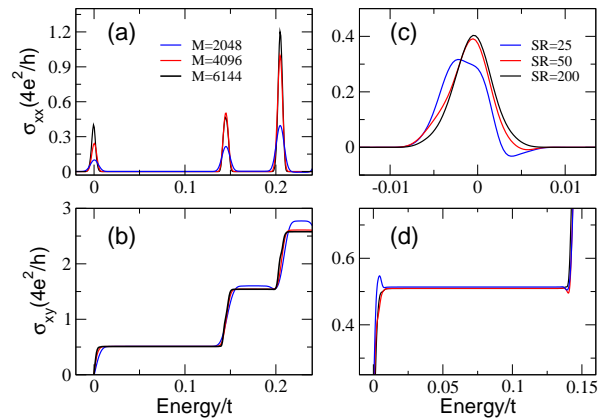


FIG. 2. Analysis of the dependency on the number of random vectors and disorder realizations SR and moments M : (a) σ_{xx} and (b) σ_{xy} for $SR = 200$ and $M = 2048$ (blue), 4096 (red) and 6144 (black). (c) σ_{xx} and (d) σ_{xy} for $M = 6144$ and $SR = 25$ (blue), 50 (red) and 200 (black). In panels (a)-(d), $\phi/\phi_0 = 5 \times 10^{-3}$, and $N = 2 \times 128 \times 1024$ sites

regions of the spectra with more available states. As can be seen in Fig. 2 (b), this results in a non-homogeneous convergence of the expansion: the plateaus located close to $E = 0$ converge for lower values of M while the higher Landau levels need more moments to converge. To ensure accurate results, we can track the global convergence of the conductivity as a function of M in a desirable energy window [33].

We also need a large SR to achieve the self-averaging condition [16]. In particular, σ_{xx} and the transition between quantum Hall plateaus are sensitive to SR as illustrated in Fig. 2 (c) and (d) and convergence is obtained for $SR > 125$. From Fig. 2, we can see that intermediate values of M and SR are enough for a qualitative analysis of $\sigma_{\alpha\beta}$. For higher accuracy one needs larger values of M , which for good convergence would also require SR to be increased.

Non-trivial topologies in the band structure can also occur in the absence of an external magnetic field. In Chern insulators, time-reversal symmetry is explicitly broken without the need of an external magnetic field. In this sense, these systems can be seen as the quantized version of the AHE that has been recently observed experimentally [38]. A simple model proposed by Haldane [25] in a honeycomb lattice provides all the key ingredients of Chern insulators. The Hamiltonian is

$$\mathcal{H} = -t \sum_{\langle i,j \rangle} c_i^\dagger c_j + t_2 \sum_{\langle\langle i,j \rangle\rangle} e^{i\phi_{ij}} c_i^\dagger c_j \pm \frac{\Delta_{AB}}{2} \sum_{i \in A/B} c_i^\dagger c_i, \quad (6)$$

where t and t_2 are nearest and next-nearest-neighbor hopping amplitudes. ϕ_{ij} is equivalent to a Peierls phase with zero total flux per unit cell. The last term is an energy offset between sublattices A and B that breaks the

inversion symmetry of the Hamiltonian, opening a gap Δ_{AB} in the band structure. For $\phi = \pi/2$ and $\Delta_{AB} = 0$, the system also presents a gap of $\Delta_T = 6\sqrt{3}t_2$, and if μ lies inside the gap, the system is a Chern insulator with $\sigma_{xy} = e^2/h$. If Δ_{AB} is continuously increased, it undergoes a quantum phase transition from a Chern insulator to a normal insulator for $\Delta_{AB} > \Delta_T$ [25]. We proceed

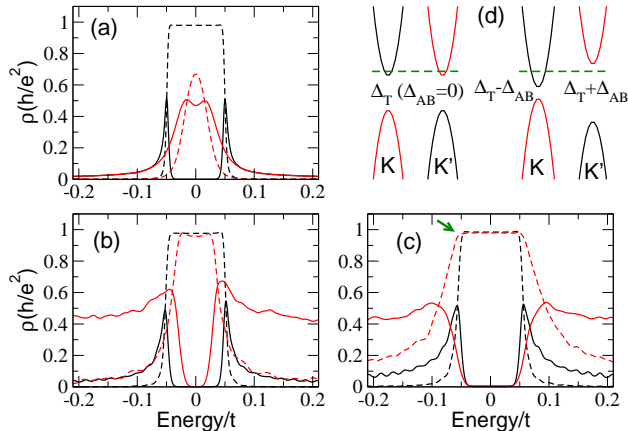


FIG. 3. ρ_{xx} (solid line) and ρ_{xy} (dashed line) for HM with (a) $\Delta_T = 0.1t$, $\Delta_{AB} = 0$ and $\gamma = 0.2t$ for $k_B T = 0$ (black) and $k_B T = 0.16t$ (red); (b) $\Delta_T = 0.1t$, $\Delta_{AB} = 0$ and $k_B T = 0$ for $\gamma = 0.4t$ (black) and $\gamma = 1.8t$ (red); (c) $\Delta_T = 0.5t$, $\Delta_{AB} = 0.4t$ and $k_B T = 0$ for $\gamma = 0.2t$ (black) and $\gamma = 1.8t$ (red). The green arrow indicates the increase of the topological region with disorder. The system sizes in panels $D = 2 \times L \times L$ with $L = 512$ (a), $L = 256$ (b-c) and $SR > 200$. Panel (d) illustrates the different gap sizes at K and K' for $\Delta_{AB} \neq 0$.

to investigate the QAHE for $\Delta_{AB} = 0$ in the presence of Anderson disorder with bounds $\pm\gamma$. As can be seen in Fig 3 (a), for weak disorder the Chern insulator is still characterized by a gap in the DOS where the Hall conductivity is quantized ($\sigma_{xy} = e^2/h$). For increasing values of T , the longitudinal and transverse resistivities are in qualitative agreement with the experimental results of Ref. [38], with the suppression of both the peak in ρ_{xy} and the dip in ρ_{xx} , supporting their findings.

A Chern insulator with a band gap Δ can be obtained by either having $\Delta_{AB} = 0$ with $\Delta_T = \Delta$ or $\Delta = \Delta_T - \Delta_{AB}$. In both situations, the QAHE leads to $\sigma_{xy} = e^2/h$ that survives to intermediate disorder strength. Surprisingly, the two systems respond differently to strong disorder: as can be seen in Fig. 3, while disorder closes the gap and destroys the Chern insulator in the system with inversion symmetry (panel b), the QAHE with $\Delta_{AB} \neq 0$ is insensitive to increasing Anderson disorder (panel c). As illustrated in panel (c), large disorder can localize carriers and extend the topological phase to energies in the vicinity of the bulk gap, similarly to what is observed in topological Anderson insulators [39, 40]. For illustration purposes, the values of Δ_T and Δ_{AB} used in panel (c) are large in comparison with values in (b). However, the same effect can be seen

if $\Delta_T > \Delta_{AB} \neq 0$. To understand this behavior, we need to compare the gaps at the Dirac points in these two situations: For $\Delta_{AB} = 0$, the two valleys are degenerate and the gaps in K and K' are both Δ_T . On the other hand, for $\Delta_{AB} \neq 0$, the interplay between Δ_T and Δ_{AB} lifts the degeneracy between valleys so that one has $\Delta = \Delta_T - \Delta_{AB}$ and the other has $\Delta = \Delta_T + \Delta_{AB}$ (see panel d). The gap difference has important consequences for the transport properties of the system. For E_F in the range $\Delta_T + \Delta_{AB} > E > \Delta_T - \Delta_{AB}$, all the states belong to K (the point group symmetry is C_3) and inter-valley scattering is forbidden as there are not available states connected to K' . This situation results in a smaller longitudinal resistivity. Also, it protects the topological gap and the QAHE as inter-valley scattering is detrimental to the state. Counter-intuitively, an asymmetry between sublattices A and B can help to stabilize the Chern insulator. In the limit of $\Delta_T = \Delta_{AB}$ the gap closes in one of the valleys, producing a state that is protected from intervalley scattering and emulates a Weyl semimetal.

In summary, we have developed a numerical method to calculate the longitudinal and transverse conductivities of tight-binding hamiltonians in real space. We illustrated the stability of the method by applying it to the QHE in disordered graphene, studying how the method's accuracy varies with the number of moments used in the expansion. To further illustrate the power of the method, we investigated the effect of disorder in the transport properties of a Chern insulator and found that due to the suppression of intervalley scattering, a Chern insulator with broken inversion symmetry is protected against scalar disorder. This finding can be useful in the search of Chern and topological insulating phases in novel materials.

The technique we have described is very general, and is suitable for the calculation of transport properties in finite temperature, disordered systems. One can simulate very large system sizes due to the method's high parallelizability that can be exploited in GPUs. Among other systems, we envisage that this method will be useful in the study of novel models with non-trivial topologies [41], spin transport in topological insulators, as well as materials without a topological phase, such as spin Hall conductivity in graphene. It can also be easily adapted to different geometries and multilayers of different materials.

We acknowledge A. R. Hernandez, A. Ferreira and E. Mucciolo for discussions. T.G.R and J.H.G acknowledge the Brazilian agencies CNPq, FAPERJ and INCT de Nanoestruturas de Carbono for financial support. L.C. acknowledges the Flemish Science Foundation (FWO-Vlaanderen) for financial support.

-
- [1] A. Bastin, C. Lewinner, O. Betbeder-Matibet and P. Nozieres, *J. Phys. Chem. Solids* **32**, 1811 (1971).
- [2] E. H. Hall, *Am. J. Math* **2**, 287 (1879).
- [3] N. Nagaosa, J. Sinova, S. Onoda, A. H. MacDonald and N. P. Ong, *Rev. Mod. Phys.* **82**, 1539 (2010).
- [4] T. Jungwirth, J. Wunderlich and K. Olejnik, *Nature Mat.* **11**, 382 (2012).
- [5] K. Klitzing, G. Dorda, M. Pepper, *Phys. Rev. Lett.* **45**, 494 (1980).
- [6] C.-Z.Chang *et al.* ,*Science* **340**,167 (2013).
- [7] M.König *et al.* , *Science* **318**, 766(2007).
- [8] M. Z. Hasan and C. L. Kane, *Rev. Mod. Phys.* **82** 3045 (2010).
- [9] R. Kubo, *J. Phys. Soc. Japan* **12**, 570 (1957); R. Kubo, A. Yokota, and S. Nakajima, *J. Phys. Soc. Japan* **12**,1203 (1957).
- [10] D.J. Thouless, M. Kohmoto, M. P. Nightingale and M. den Nijs, *Phys. Rev. Lett.* **49**, 405 (1982).
- [11] Yisong Zheng and Tsuneya Ando, *Phys. Rev. B* **65**, 245420 (2002).
- [12] D. N. Sheng, L. Sheng, and Z. Y. Weng, *Phys. Rev. B* **73**, 233406 (2006).
- [13] Yu Xue and Emil Prodan, *Phys. Rev. B* **86**, 155445 (2012).
- [14] Frank Ortmann and Stephan Roche, *Phys. Rev. Lett.* **110**, 086602 (2013).
- [15] D. A. Greenwood, *Proc. Phys. Soc. (London)* **71**, 585 (1958).
- [16] A. Weisse, G. Wellein, A. Alvermann, H. Fehske, *Rev. Mod. Phys.* **78**, 275(2006).
- [17] S. Roche, *Phys. Rev. B* **59**, 2284 (1999).
- [18] S. Yuan, H. De Raedt, and M.I. Katsnelson, *Phys. Rev. B* **82**, 115448 (2010).
- [19] Aires Ferreira, J. Viana-Gomes, Johan Nilsson, E. R. Mucciolo, N. M. R. Peres, and A. H. Castro Neto, *Phys. Rev. B* **83**, 165402 (2011).
- [20] Z. Fan, A. Uppstu, T. Siro, and A. Harju, *Computer Physics Communications* **185**, 28 (2014).
- [21] T. L. van den Berg, L. Raymond, A. Verga, *Phys. Rev. B* **84**, 245210 (2011).
- [22] A. H. Castro Neto, F. Guinea, N. M. R. Peres, K. S. Novoselov, and A. K. Geim, *Rev. Mod. Phys.* **81**, 109 (2009).
- [23] S. Das Sarma, Shaffique Adam, E. H. Hwang, Enrico Rossi, *Rev. Mod. Phys.* **83**, 407 (2011) and references therein.
- [24] S. Gattenlohner, W.-R. Hanne, P. M. Ostrovsky, I. V. Gornyi, A. D. Mirlin, M. Titov, *Phys. Rev. Lett.* **112**, 026802 (2014)
- [25] F. D. M. Haldane, *Phys. Rev. Lett.* **61**, 2015 (1988).
- [26] A. Crepieux, and P. Bruno, *Phys. Rev. B* **64**, 094434 (2001).
- [27] P. Streda, *J. Phys. C: Solid State Phys.* **15**, L717 (1982); **15**, L1299 (1982).
- [28] R.N. Silvera, H. Roederb, A.F. Votera, J.D. Kressb, *Journal of Computational Physics* **124**, 115 (1996).
- [29] L. Covaci, F.M. Peeters, M. Berciu, *Phys. Rev. Lett.* **105**, 167006 (2010)
- [30] M. Ganahl, P. Thunstrom, F. Verstraete, K. Held, H. G. Evertz, *Phys. Rev. B.* **90**, 045144 (2014).
- [31] F. A. Wolf, Ian P. McCulloch, Olivier Parcollet, and Ulrich Schollwock, *Phys. Rev. B.* **90**, 115124 (2014).
- [32] "Numerical Analysis: Mathematics of Scientific Computing, Vol 2", David Ronald Kincaid, Elliott Ward Cheney, American Mathematical Society (2002).
- [33] See Supplemental Material [url], which includes Refs. [42-48]
- [34] A. Weisse, *Eur. Phys. J. B* **40**, 125 (2004); A. Weisse, G. Schubert, H. Fehske, *Physica B* **359-361**, 786 (2005).
- [35] R. Alben, M. Blume, H. Krakauer, L. Schwartz, *Phys.Rev. B* **12**, 4090(1975).
- [36] Toshiaki Iitaka, Toshikazu Ebisuzaki, *Phys. Rev. E*,**69**, 057701(2004).
- [37] K. S. Novoselov, A. K. Geim, S. V. Morozov, D. Jiang, M. I. Katsnelson, I. V. Grigorieva, S. V. Dubonos, and A. A. Firsov, *Nature* **438**, 197 (2005).
- [38] C. Z. Chang *et al.* *Science* **340** 167 (2013).
- [39] Jian Li, Rui-Lin Chu, J. K. Jain, and Shun-Qing Shen, *Phys. Rev. Lett.* **102**, 136806 (2009).
- [40] Juntao Song, Haiwen Liu, Hua Jiang, Qing-feng Sun, and X. C. Xie, *Phys.Rev. B* **85**, 195125 (2012).
- [41] K. Sun, Z. Gu, H. Katsura, and S. Das Sarma, *Phys. Rev. Lett.* **106**, 236803 (2011); E. Tang, J.-W. Mei, and X.-G. Wen, *Phys. Rev. Lett.* **106**, 236802 (2011); T. Neupert, L. Santos, C. Chamon, and C. Mudry, *Phys. Rev. Lett.* **106**, 236804 (2011).
- [42] Holger Fehske, Jens Schleede, Gerald Schubert, Gerhard Wellein, Vladimir S. Filinov, Alan R. Bishop, *Phys. Lett. A* **373**, 2182 (2009).
- [43] J. B. Wang and T. T. Scholz , *Phys. Rev. A* **57**, 3554 (1998).
- [44] A. Weisse and H. Fehske, *Lect. Notes Phys.* **739**, 545577 (2008).
- [45] D. Jackson, American Mathematical Society Colloquium Publications D. Jackson, **XI** providence R. I. (1930).
- [46] D. A. Drabold and O. F. Sankey, *Phys. Rev. Lett.* **70** 3631(1993).
- [47] Silver, R. N., and H. Rder *Int. J. Mod. Phys. C* **5** 935 (1994).
- [48] Cuda Perfomance Report, September 2014.

Supplementary Material for "Real-space calculation of the conductivity tensor for disordered topological matter"

In this supplementary material, we show in detail how the kernel polynomial method (KPM) can be used to calculate $\sigma_{\alpha,\beta}(\mu)$ in an efficient and scalable way for all energies and temperatures. For consistency, let us first review some basic information about the KPM. This method works by expanding a spectral operator of interest $\Lambda(\varepsilon, H)$ in terms of the Chebyshev polynomials of first kind

$$T_m(x) \equiv \cos(\arccos(x)), \quad T_{m+1}(x)$$

. For this purpose, the Hamiltonian needs to be rescaled so that its energy spectrum is contained in the $[-1,1]$ interval. This can be done by rescaling the Hamiltonian and energies in the following way:

$$\tilde{H} = \frac{2}{\Delta E} \left(H - \frac{E^+ + E^-}{2} \right), \quad \tilde{\varepsilon} = \frac{2}{\Delta E} \left(\varepsilon - \frac{E^+ + E^-}{2} \right), \quad (7)$$

where $E^+(E^-)$ is the higher (lower) bound of the spectra and $\Delta E = E^+ - E^-$. To expand the scaled spectral quantity $\tilde{\Lambda}(\tilde{\varepsilon}, \tilde{H})$ we use the spectral representation

$$\tilde{\Lambda}(\tilde{\varepsilon}, \tilde{H}) = \sum_k \tilde{\Lambda}(\tilde{\varepsilon}, \tilde{E}_k) \left| \tilde{E}_k \right\rangle \left\langle \tilde{E}_k \right|, \quad (8)$$

where $\tilde{H} \left| \tilde{E}_k \right\rangle = \tilde{E}_k \left| \tilde{E}_k \right\rangle$ and expand each of the functions as follows:[1]

$$\tilde{\Lambda}(\tilde{\varepsilon}, \tilde{E}_k) = \frac{2}{\pi} \sum_{m=0}^{\infty} \Gamma_m(\tilde{\varepsilon}) T_m(\tilde{E}_k), \quad \Gamma_m(\tilde{\varepsilon}) = \frac{1}{\delta_{m,0} + 1} \int_{-1}^1 \frac{\tilde{\Lambda}(\tilde{\varepsilon}, \tilde{E}_k) T_m(\tilde{E}_k)}{\sqrt{1 - \tilde{E}_k^2}} d\tilde{E}_k, \quad (9)$$

where the Chebyshev polynomials can be efficiently evaluated by means of the recursion relationship $T_m(x) = 2xT_{m-1}(x) - T_{m-2}(x)$. Finally, by inserting the above expression into (8) we obtain the expansion for the spectral operator

$$\tilde{\Lambda}(\tilde{\varepsilon}, \tilde{H}) = \frac{2}{\pi} \sum_{m=0}^{\infty} \Gamma_m(\tilde{\varepsilon}) T_m(\tilde{H}), \quad (10)$$

where now all the information associated to the form of Λ had been separated from the information associated with the Hamiltonian. This type of expansion was used to approximate spectral operators such as the Greens functions [2] and the evolution operator[3, 4]. In many cases, only part of the information contained in the Hamiltonian is needed. This is for example the case of the partition function \mathcal{Z} and the density of states $\rho(\varepsilon)$ [1, 5], which depends only on the trace of H . As an example, we can consider $\tilde{\rho}(\tilde{\varepsilon})$ where $\tilde{\Lambda}(\tilde{\varepsilon}, \tilde{H}) = \delta(\tilde{H} - \tilde{\varepsilon})$ and (10) becomes

$$\tilde{\rho}(\tilde{\varepsilon}) = \frac{2}{\pi\sqrt{1 - \tilde{\varepsilon}^2}} \sum_{m=0}^{\infty} \Gamma_m(\tilde{\varepsilon}) \mu_m, \quad (11)$$

where $\Gamma_m(\tilde{\varepsilon}) = T_m(\tilde{\varepsilon})$ and $\mu_m \equiv \text{Tr}[T_m(\tilde{H})]$, obtained in 5 by expanding the δ -function directly. The equation (11) is the general form of the trace of an arbitrary spectral operator and the expansion is exact. However, in practice it is always necessary to truncate the series at some finite order M and experience shows that this truncation can produce poor precision and Gibbs oscillations, specially in points where the function is not continuously differentiable. One way to reduce finite order problems is to modify the moments $\mu_m \rightarrow g_m \mu_m$ with the use of a kernel, that basically smooth the problematic points. The Jackson Kernel,

$$g_m^J = \frac{(M - m + 1) \cos \frac{\pi m}{M+1} + \sin \frac{\pi m}{M+1} \cot \frac{\pi}{M+1}}{M + 1}, \quad (12)$$

has been extensively tested and studied [1, 6, 7] and it is one of the best kernels for spectral quantities, as it has the advantage of being positive and normalized. Consequently, it preserves the positiveness and the value of the integration of the approximated function. Calculating the trace of all $\text{Tr}[T_m(H)]$ can be a difficult task for large matrices. Fortunately, there is a method, known as random phases vector approximation [1, 8, 9], to calculate the

traces that takes advantage of the size N of the matrices. In this method we construct a set of vectors of $R \ll N$ complex vectors

$$|r\rangle \equiv (\xi_1^r, \dots, \xi_N^r), \quad r = 1, \dots, R, \quad (13)$$

with dimension equal to N and whose elements ξ_i^r are drawn from a probabilistic distribution with the following characteristics:

$$\langle\langle \xi_i^r \rangle\rangle = 0, \quad \langle\langle \xi_i^{r*} \xi_j^{r'} \rangle\rangle = \delta_{r,r'} \delta_{i,j}, \quad (14)$$

where $\langle\langle \dots \rangle\rangle$ is the statistical average. The trace can be calculated as the average expected value of this random vector,

$$\text{Tr} [T_m(\tilde{H})] \approx \frac{1}{R} \sum_{r=1}^R \langle r | T_m(\tilde{H}) | r \rangle. \quad (15)$$

The error of this approximation is $\mathcal{O}(1/\sqrt{RN})$, therefore it is reduced when increasing N or R and for very large system only a few random vectors are necessary. In principle, it is possible to use any distribution function that satisfies the conditions of Eq. (14). However, it was prove that choosing $\xi_i^r = e^{i\phi}/N$, with ϕ as a random variable uniformly distributed in the interval $(0, 2\pi)$ reduces the statistical error, therefore the convergence is improved [9, 10].

Now that we presented the basics of the KPM, we can proceed to expand the conductivity tensor $\sigma_{\alpha,\beta}(\mu)$. Our starting point is the the formula given by Bastin *et al.* [11] with the assumption that the Hamiltonian has finite lower and upper bounds, which is always true for a tight-binding Hamiltonian:

$$\sigma_{\alpha\beta}(\mu) = \frac{ie^2\hbar}{\Omega} \int_{E^-}^{E^+} d\varepsilon f(\varepsilon) \text{Tr} \left\langle v_\alpha \delta(\varepsilon - H) v_\beta \frac{dG^+(\varepsilon, H)}{d\varepsilon} - v_\alpha \frac{dG^-(\varepsilon, H)}{d\varepsilon} v_\beta \delta(\varepsilon - H) \right\rangle. \quad (16)$$

Here, Ω is the volume, $G^\pm(\varepsilon, H)$ are the advanced and retarded Green functions, v_α is the velocity operator in the α direction and $f(\varepsilon)$ is the Fermi-Dirac distribution for a given chemical potential μ and temperature T . We begin by rescaling of the Hamiltonian $H \rightarrow \tilde{H}$ and the energies $\varepsilon \rightarrow \tilde{\varepsilon}$ and replace them in the Bastin's Formula

$$\begin{aligned} \sigma_{\alpha\beta}(\mu) &= \left(\frac{2}{E^+ - E^-} \right)^2 \frac{ie^2\hbar}{\Omega} \int_{-1}^1 d\tilde{\varepsilon} f(\tilde{\varepsilon}, \tilde{\mu}) \text{Tr} \left\langle v_\alpha \delta(\tilde{\varepsilon} - \tilde{H}) v_\beta \frac{dG^+(\tilde{\varepsilon}, \tilde{H})}{d\tilde{\varepsilon}} - v_\alpha \frac{dG^-(\tilde{\varepsilon}, \tilde{H})}{d\tilde{\varepsilon}} v_\beta \delta(\tilde{\varepsilon} - \tilde{H}) \right\rangle \\ \sigma_{\alpha\beta}(\mu) &= \left(\frac{2}{E^+ - E^-} \right)^2 \tilde{\sigma}_{\alpha\beta}(\tilde{\mu}), \end{aligned} \quad (17)$$

so we can work with the rescaled conductivity $\tilde{\sigma}_{\alpha,\beta}(\tilde{\mu})$. Using the expression (10), we can expand both the δ and the Green function in terms of the Chebyshev polynomials

$$\delta(\tilde{\varepsilon} - \tilde{H}) = \frac{2}{\pi\sqrt{1-\tilde{\varepsilon}^2}} \sum_{m=0}^{\infty} T_m(\tilde{\varepsilon}) T_m(\tilde{H}), \quad G^\pm(\tilde{\varepsilon}, \tilde{H}) = \mp \frac{2i}{\sqrt{1-\tilde{\varepsilon}^2}} \sum_{m=0}^M g_m e^{\pm i m \arccos(\tilde{\varepsilon})} T_m(\tilde{H}). \quad (18)$$

By replacing the functions above in (16) we have

$$\tilde{\sigma}_{\alpha\beta}(\tilde{\mu}) = \frac{4e^2\hbar}{\pi\Omega} \int_{-1}^1 \frac{d\tilde{\varepsilon} f(\tilde{\varepsilon})}{(1-\tilde{\varepsilon}^2)^2} \sum_{m,n} \mu_{nm}^{\alpha\beta} \Gamma_{nm}(\tilde{\varepsilon}), \quad (19)$$

where

$$\mu_{mn}^{\alpha\beta} \equiv \frac{g_m g_n}{(1+\mu_{n0})(1+\mu_{m0})} \text{Tr} [v_\alpha T_m(\tilde{H}) v_\beta T_n(\tilde{H})], \quad (20)$$

does not depend of $\tilde{\varepsilon}$ and carries all the information about the system, being also responsible for most of the computational cost. On the other hand,

$$\Gamma_{mn}(\tilde{\varepsilon}) \equiv \left(\varepsilon - in\sqrt{1-\varepsilon^2} \right) T_m(\varepsilon) e^{i m \arccos(\varepsilon)} + \left(\varepsilon + im\sqrt{1-\varepsilon^2} \right) T_n(\varepsilon) e^{-i m \arccos(\varepsilon)}, \quad (21)$$

is independent of the Hamiltonian and can be thought as the expansion basis. (19) can be seen as a generalization of (11) where more than two spectral functions are present in the expansion. By using the properties

$$(\mu_{mn}^{\alpha\beta})^* = \mu_{nm}^{\alpha\beta} = \mu_{mn}^{\beta\alpha} \quad \text{and} \quad \Gamma_{mn}^* = \Gamma_{nm}, \quad (22)$$

it is possible to write the conductivity as a complete real quantity

$$\tilde{\sigma}_{\alpha\beta}(\mu) = \frac{4e^2\hbar}{\pi\Omega} \int_{-1}^1 \frac{d\tilde{\varepsilon} f(\tilde{\varepsilon})}{(1-\tilde{\varepsilon}^2)^2} \sum_{m,n \leq m} \text{Re} [\mu_{nm}^{\alpha,\beta} \Gamma_{nm}(\tilde{\varepsilon})]. \quad (23)$$

Finally, as an example of the consistency of our approach, we integrate this equation analytically to obtain the Kubo-Greenwood formula for the longitudinal conductivity. For this purpose we can use (22) to show that $\mu_{mn}^{\alpha\alpha}$ is real and therefore $\text{Re} [\mu_{nm}^{\alpha\alpha} \Gamma_{n,m}(\tilde{\varepsilon})] = \mu_{nm}^{\alpha\alpha} \text{Re} [\Gamma_{nm}(\tilde{\varepsilon})]$. Taking this into account, we can write

$$\tilde{\sigma}_{\alpha\alpha}(\tilde{\mu}) = \frac{4e^2\hbar}{\pi\Omega} \sum_{m,n \leq m} \mu_{nm}^{\alpha\alpha} \int_{-\alpha}^{\alpha} \frac{d\tilde{\varepsilon} f(\tilde{\varepsilon})}{(1-\tilde{\varepsilon}^2)^2} \left(\frac{d}{d\tilde{\varepsilon}} [\text{T}_n(\tilde{\varepsilon})\text{T}_m(\tilde{\varepsilon})] + 2\tilde{\varepsilon}\text{T}_n(\tilde{\varepsilon})\text{T}_m(\tilde{\varepsilon}) \right), \quad (24)$$

that can be integrated analytically for $T = 0$:

$$\sigma_{\alpha\alpha}(\tilde{\varepsilon}_F) = \frac{4e^2\hbar}{\pi\Omega} \sum_{m,n \leq m} \mu_{nm}^{\alpha\alpha} \text{T}_n(\tilde{\varepsilon}_F) \text{T}_m(\tilde{\varepsilon}_F), \quad (25)$$

which is the Kubo-Greenwood formula expressed in terms of the Chebyshev Polynomials as shown in [1].

Convergence of the method

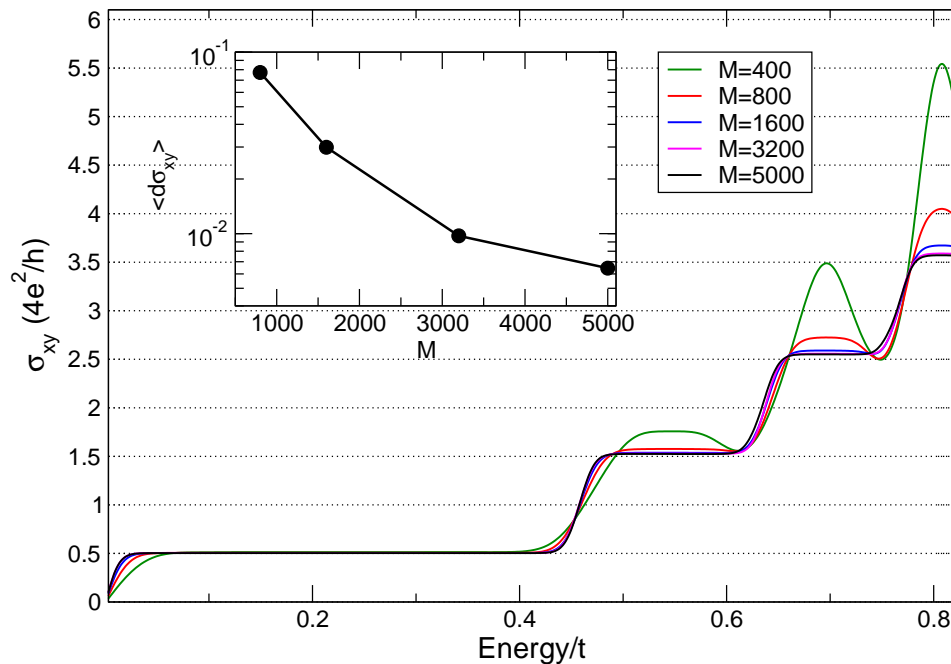


FIG. 4. σ_{xy} as a function of E for increasing values of M . $\phi/\phi_0 \approx 1 \times 10^{-2}$, $SR > 150$, $K_B T = 0.005t$ and $N = 2 \times 400 \times 400$ sites. Inset: $\langle d\sigma_{xy}(E) \rangle$ as a function of M for the data shown in the main panel.

In the figure 1, we illustrate how we track the convergence in function of M : in this particular case, we choose the window $(0, 0.8t]$ in energy and calculate $\sigma_{xy}(E)$ for two different values of M ($M' < M$). We then obtain

$$\langle d\sigma_{xy}(E) \rangle = \left\langle \left| \frac{\sigma_{xy}^M(E) - \sigma_{xy}^{M'}(E)}{\sigma_{xy}^M(E)} \right| \right\rangle_E,$$

where we calculate the discrepancy between the conductivity for different values of M at each energy point and average over the energy. In the inset, we can see that for $M = 5000$, $\langle d\sigma_{xy}(E) \rangle < 10^{-2}$ which means that further increases in the number of moments of the expansion will provide very small changes in the conductivity. The conductivity converges slowly for large values of M ($\langle d\sigma_{xy}(E) \rangle \propto M^{-1.4}$) and for increasing values of M , the changes will mostly occur at high energies. If we choose a different window of energy, as for example $(0, 0.4t]$, $\langle d\sigma_{xy}(E) \rangle < 10^{-3}$ even for $M = 3200$. We then truncate our expansion for $\langle d\sigma_{xy}(E) \rangle \sim 10^{-2}$.

A similar analysis can be performed with the number of random vectors R , as shown in figure 2. For R , we consider $\langle d\sigma_{xy}(E) \rangle \sim 10^{-3}$. Our general procedure is to converge SR for each value of M for a given energy range and then look at the convergence as a function of M . It is important to mention that for increasing values of M , convergence requires increasing values of SR . However, temperature reduces small fluctuations in the conductivity that arise from the use of few random vectors, eliminating the need of large SR for finite T .

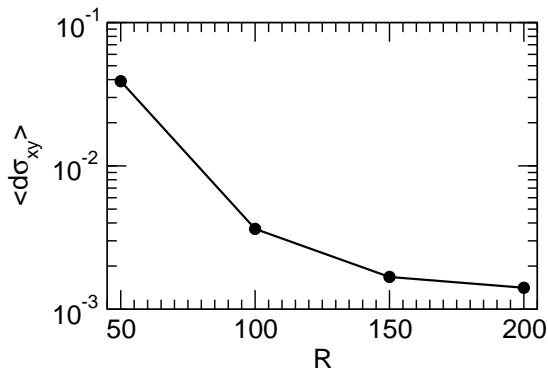


FIG. 5. (a) $\langle d\sigma_{xy}(E) \rangle$ as a function of R for $\phi/\phi_0 \approx 1 \times 10^{-2}$, $M = 3200$, $k_B T = 0$ and $N = 2 \times 400 \times 400$ sites.

The Hall conductivity presents deviations from the quantized value for high energies. However, if we look at the values of the quantized changes in σ_{xy} in the figure below ($M = 5000$), for positive n we have 1.015, 1.025, 1.03, 1.03, 1.06 in units of $4e/h^2$. The contribution of each Landau level to the Hall conductivity has an error or the order of 1-5 %. However, the error in the conductivity accumulates and deviates from the expected values at high LL levels. The small increase of the error with energy is related with the convergence with M discussed above.

GPU Computing

As discussed in the previous section, the main computational cost of our approach is the calculation of elements such as $T_m(\tilde{H})|r\rangle$ with $T_m(\tilde{H}) = 2\tilde{H}T_{m-1}(\tilde{H}) - T_{m-2}(\tilde{H})$. For a conductivity calculation with $M = 10^3$ it is necessary to calculate around 10^6 matrix-vector products, with matrices of dimension $N \times N$ and $N \approx 10^5 - 10^7$. To reduce the computational time, we take advantage of the fact that the real space tight-binding Hamiltonians are represented by sparse matrices, so we write the matrix in a sparse format which greatly reduces the computational cost from $\mathcal{O}(N^2) \rightarrow \mathcal{O}(N)$. We take advantage of the parallel nature of Graphics Processing Units (GPU) to compute these products in a very efficient way. We perform our simulations in CUDA, NVIDIA proprietary parallel computing platform. We also use NVIDIA CUDA Sparse Matrix library (cuSPARSE) that provides basic linear algebra subroutines used for sparse matrices and CUSP, another Sparse Matrix library for CUDA. The performance of these packages had been tested by NVIDIA and achieves a speedup of roughly 10 times of a common CPU with MKL optimized libraries[12].

-
- [1] Alexander Weisse, Gerhard Wellein, Andreas Alvermann and Holger Fehske, Rev. Mod. Phys. **78**, 275 (2006).
 - [2] L. Covaci, F. M. Peeters and M. Berciu, Phys. Rev. Lett. **105**, 167006 (2010).
 - [3] Holger Fehske, Jens Schleede, Gerald Schubert, Gerhard Wellein, Vladimir S. Filinov, Alan R. Bishop, Phys. Lett. A **373**, 2182 (2009).
 - [4] J. B. Wang and T. T. Scholz, Phys. Rev. A **5**, 57 (1998).
 - [5] R. N. Silver, H. Roeder, A. F. Voter and J. D. Kress, Journal of Computational Physics **124**, 115-130 (1996).
 - [6] A. Weisse and H. Fehske, Lect. Notes Phys. **739**, 545577 (2008).

- [7] D. Jackson, American Mathematical Society Colloquium Publications D. Jackson, **XI** providence R. I. (1930).
- [8] D. A. Drabold and O. F. Sankey, Phys. Rev. Lett. **70** 3631(1993).
- [9] Silver, R. N., and H. Rder Int. J. Mod. Phys. C **5** 935 (1994).
- [10] Toshiaki Iitaka and Toshikazu Ebisuzakis, Phys. Rev. E **69** 057701 (2004).
- [11] A. Bastin, C. Lewiner, O. Betbeder-Matibet et P. Nozieres, J. Phys, Chem. Solids **32** 1-1824 (1971).
- [12] Cuda Perfomance Report, September 2014.